CHAPTER-3

Metal Nanoparticles (MNPs)-Decorated Reduced graphene oxide nanosheets as efficient catalysts for Hydrogenolysis of Benzyl Alcohol

[3.1] Introduction

Homogeneous and heterogeneous catalytic processes play a crucial role in the chemical transformation owing to focusing on both economical success and environmental sustainability [1–3]. However, homogeneous catalysts are suffering from high cost and laborious catalyst separation which lead to serious economical and environmental problems [4–7]. To overcome this troublesome, heterogenenization of these homogeneous catalysts has been carried out because it is regenerable, easy to handle, tolerates a wide range of temperature and pressure, drop down of waste, and also employed in up-scale reactions [8–11]. The traditional heterogeneous catalysts are laboring from moderately low activities as well and hence great efforts are being put to affix them onto the solid supports. A variety of solid supports including activated carbon [12], carbon nanotubes [13], alumina [14], silica [15], zeolites [16], clays [17] and zinc ferrite [18] have been developed to date. Amongst these, carbonaceous materials especially graphene preferred widely due to its abundance, light weight, densely packed hexagonal honeycomb sp^2 hybridized 2D lattice, exceptional large surface area (2630 m^2g^{-1}), high electrical conductivity and thermal stability as well as inertness to supported metals [19–24].

Since 21st century, metal nanoparticles (MNPs), due to their distinctive properties and wide potential applications such as drugs and medications, chemical sensors and biosensors, paint-pigments, cosmetics, pharmaceuticals, catalysis and supports, magnetic and optical devices, batteries and fuel cells, electronic and magnetic devices, structured materials and protective coatings have increasingly gained influence [25–33]. Currently, transition metals and metal oxides with plenty of availability, low cost, high thermal capacity and remarkable electron charge transfer properties, play a crucial role in catalysis. Despite of these advantages, they endures from some difficulties like re-dispersion, sintering snags, agglomeration owing to its small particle size and also thermodynamic instability which results in deactivation and lose in activity. Moreover, metal and metal oxides can easily and uniformly be dispersed on graphene nanosheet and

the charge transfer at the interface which provide synergistic effect considerably improving their catalytic activity [34].

The catalytic hydrogenolysis of benzyl alcohol (BzA) bestows the industrially important product such as methylene compounds by signifying the desirable pathway for the reductive cleavage of carbon-oxygen bond. The flexibility of $Et_3SiH/PdCl_2$ system was demonstrated by Mirza-Aghayan and his co-workers [35] for the selective reduction of carbonyl groups of aromatic aldehydes and ketones into a methylene group. In another work this group [36] have synthesized palladium nanoparticles supported on reduced graphene oxide (Pd NPs/rGO) using a sonochemical procedure and was checked for reduction of benzyl alcohol derivatives into the corresponding methylene compounds in the presence of Et_3SiH.

Now-a-days, researchers have gradually focused on the development of new-fangled, inexpensive, and more efficient metal nanoparticle based catalyst that leads to hydrogenolysis reaction at ambient condition and by doing it can help in decrease the generation of pollutants. According to literature survey, a variety of heterogeneous catalysts comprising noble metals such as Pd, Pt, Rh, Ag and Au [37,38] have been developed for hydrogenolysis reaction. However, this reaction involved the use of hazardous hydrogen gas. Moreover, other disadvantages of this noxious gas is its high price, formation of undesired product, requirement of high pressure and higher equipment and more energy input make the use of stoichiometric amounts of the reducing agents obligatory as well. Many reducing agents are accessible in this modern age such as sodium borohydride, tributylstannane, hydrazine hydrate, formaldehyde, organosilanes etc. However, amongst them, organosilanes is less ionic, less toxic and hence used in an environmentally benign process. Besides these advantages, due to their low capacity to donate hydrogen atoms, it suffers as poor reducing agent. To overcome these drawbacks, a numerous chemically functionalized silanes with weaker Si–H bonds and composite reducing systems have been developed based on amalgamation of silane with transition metal catalyst [39,40]. These fresh fused silane/transition metal catalyst have been utilized for several reactions such

as the reduction of Schiff bases [41], selective dehydroxylation of secondary benzylic alcohols [42], and direct catalytic deoxygenation of propargyl alcohols [43]. The efficiency of $Et_3SiH/PdCl_2$ catalytic system for various organic transformations [44], including the reduction of aromatic carbonyl compounds [45].

Based on the above observations, the present work was aimed at exploring the catalytic efficacy of more proficient and cheap MNPs@rGO catalysts (where M= VO, Ni and Cu) towards the hydrogenolysis of BzA proceeds through in situ generated molecular hydrogen at room temperature using (Et_3SiH) as a reducing agent and dry ethanol as a solvent. The best suited catalyst for this transformation was chosen by optimization of various parameters, for instance, various mole ratio, catalyst amount, time, solvent and temperature, etc.

[3.2] Experimental section

a) Materials

Triethylsilane (Et_3SiH) was procured from Spectrochem And Other chemicals such as benzyl alcohol, $Cu(NO_3)_2 \cdot 3H_2O$, $VOSO_4.5H_2O$, $Ni(NO_3)_2.6H_2O$, l-ascorbic acid were purchased from S D Fine-Chem Ltd. All the materials are of analytical grade and used as received without further purification.

b) Synthesis of GO

GO was synthesized from graphite flakes using a modified Hummers' method as discussed in chapter 2.

c) Synthesis of rGO

rGO was prepared GO via the chemical reduction method as discussed in chapter 2.

d) Synthesis of MNPs@rGO nanocomposites

As-prepared GO (10 mg) was suspended into deionized water (15 mL) followed by drop-wise addition of 2 mmol metal salt solutions [$Cu(NO_3)_2.3H_2O$, $VOSO_4 \cdot 5H_2O$, and/or $Ni(NO_3)_2.6H_2O$] and ultrasonicated for 20 min to produce homogeneously dispersed suspension. A freshly prepared solution of l-ascorbic acid (5 mL) was added drop-wise into suspension with constant stirring and

heated at 90 ^{o}C for 4 h. The obtained black precipitates signify the successful reduction of both metal salts and GO. The excess ascorbic acid can be removed from the product using H_2O_2. The solid product was separated by centrifugation followed by washed with ethanol and deionized water and finally dried in an air oven at 65 ^{o}C

e) Catalytic hydrogenolysis of BzA

In a typical hydrogenolysis reaction, a mixture of 1 mmol BzA, 2 mmol Et_3SiH, 5 mL dry ethanol and 10 mg catalyst were added into a three-necked 50 mL round bottle flask at ambient temperature and the reaction mixture were kept under vigorous stirring for 10 min under argon atmosphere. After completion of the reaction, the solid catalyst was separated from the reaction mixture by centrifugation and washed with ethyl acetate. The organic aliquot was analyzed by a Chemito 8610 gas chromatography (GC) equipped with a flame ionization detector and a DB-5 capillary column (30 m, 0.32 mm id, 0.25 μm film thickness).

[3.3] Results and discussion

The schematic diagram for the synthesis of chemically-derived MNPs@rGO catalysts is shown in Scheme 1. These catalysts were characterized by various physicochemical techniques are discussed here.

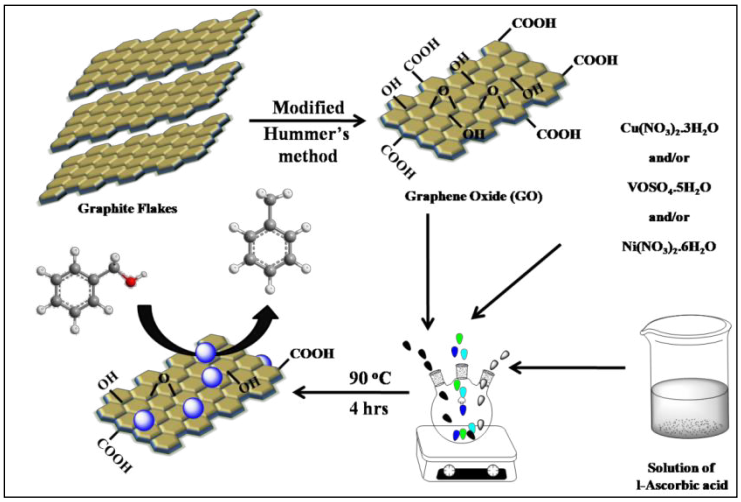

Scheme 1. Synthesis of chemically-modified MNPs@rGO catalysts.

a) Transmission electron microscopy:

The surface morphology and structural property of CuNPs@rGO nanocomposite have been substantiated by transmission electron microscopy (TEM). From Fig.1 (a) and (b), it can be examined that the fine narrow-sized Cu nanoparticles (CuNPs) were dispersed on the rGO nanosheets. The size distribution of the CuNPs on the rGO nanosheets was calculated by ImageJ software, where, the average size of the nanoparticles was found 3.6 ± 1.1 nm.

Besides, it can be seen that the rGO surface has some wrinkled regions and the scrolled edges, which causes good stabilization of MNPs and also avoids the agglomeration or aggregation. As can be seen in Fig. 1 (e), the polycrystalline nature of CuNPs has been confirmed by the existence of diffraction dots in the selected area diffraction pattern (SAED). However, intense spherical spots correspond to (111), (200) and (220) planes of cubic phase [47], which is in good agreement with the XRD results as discussed below.

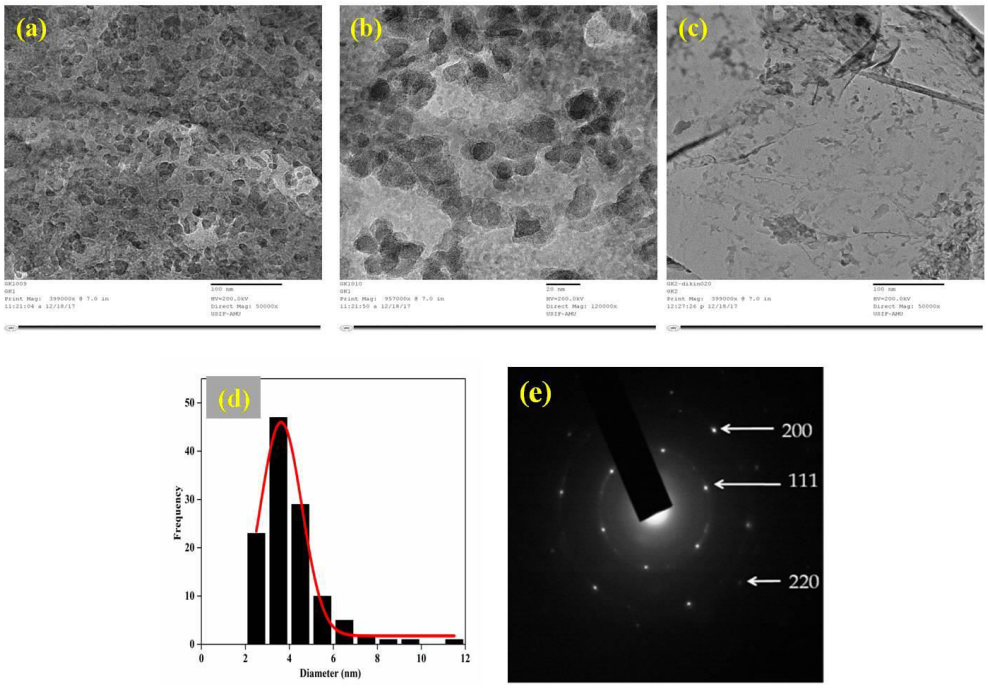

Figure 1. TEM images of (a, b, and c) CuNPs@rGO, (d) Average size of nanoparticle and (e) SAED image of CuNPs@rGO.

b) X-ray Diffraction Patterns:

Successful formation of metal nanoparticles on rGO nanosheet was confirmed by powder X-ray diffraction patterns (fig. 2). We have also quantified interlayer distance of GO before and after reduction process by XRD pattern (described in Chapter 2, fig. 8). The XRD pattern of CuNPs@rGO, VONPs@rGO and NiNPs@rGO (fig. 2) were observed at about 24°, indicating the effective reduction of GO into rGO. [48].

This result suggests the formation of new in-plane sp^2 domains during reduction process which is in accordance with Raman and XPS results as discussed later. Furthermore, in the spectra of CuNPs@rGO, VONPs@rGO and NiNPs@rGO (fig. 2 (a, b, c)), three diffraction peaks located at 42.92°, 51.43° and 74.76° were assigned to (111), (200) and (220) crystallographic planes of cubic MNPs, respectively. In addition, we have checked the nanocrystalline size of the as-prepared MNPs@rGO catalysts by employing Scherer equation. The approximate size calculated was 3-6 nm, which is in good concurrence with the TEM results.

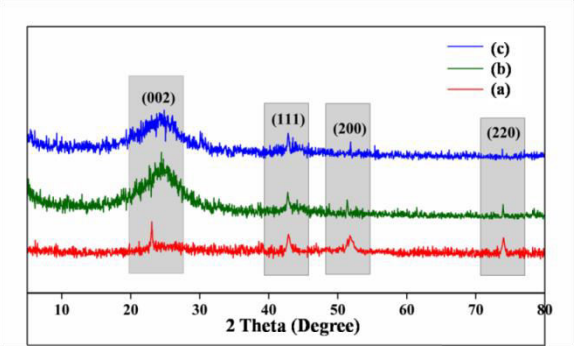

Figure 2. X-ray diffraction patterns of (a) CuNPs@rGO (b) VONPs@rGO and (c) NiNPs@rGO.

c) Raman Spectroscopy:

Raman spectroscopy is a powerful non-destructive technique to evaluate the disorder and defect structures in graphene-based materials. The Raman spectra of GO as described in Chapter 2, Fig. 10, which is compared with the Raman

spectra of CuNPs@rGO, NiNPs@rGO and VONPs@rGO nanocomposite materials (fig. 3).

In these spectra, two prominent peaks were detected at ~1348 cm^{-1} (D Band appeared due to the A_{1g} breathing mode of disordered graphite structure) and ~1585 cm^{-1} (G Band appeared due to the scattering of E_{2g} phonons of sp^2 carbon atoms). The intensity ratio of D/G band which is a measure of the defects present on the graphene structure was increased to 1.11 for CuNPs@rGO, 1.06 for NiNPs@rGO and 1.23 for VONPs@rGO, respectively, which all are correspond to the GO (chapter 2, fig. 10). This increment was might be due to the increase in defects of the rGO sheet which suggests the successful reduction of GO and formation of new in-plane sp^2 domains during reduction process [49]

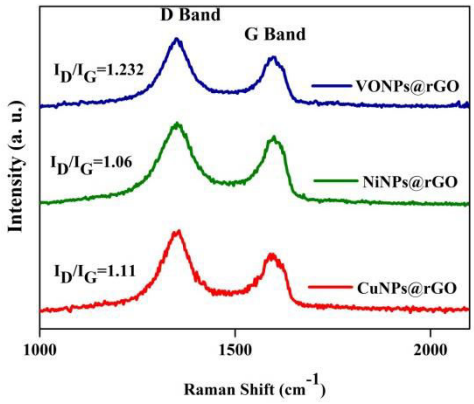

Figure 3. Raman spectra of GO, CuNPs@rGO, NiNPs@rGO and VONPs@rGO.

d) FTIR spectra:

The FTIR spectra of GO and rGO as shown in chapter 2, fig. 6, which is matched with CuNPs@rGO, NiNPs@rGO and VONPs@rGO (fig. 4)

In the FTIR spectra of CuNPs@rGO, NiNPs@rGO and VONPs@rGO, the disappearance of peaks (i.e. 1732 and 1040 cm^{-1}) were observed, which evidently signifies the successful removal of carbonyl and alkoxy groups, respectively. However, in all the spectra of CuNP@rGO, NiNPs@rGO and VONPs@rGO, one prominent peak at 1220 cm^{-1} due to epoxy group was remain

intact even after reduction process, which indicates that the epoxy group does not affected during the reduction process [50].

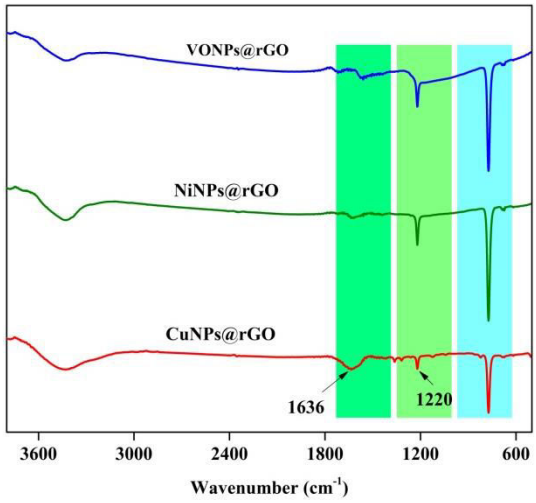

Figure 4. The FTIR spectra of CuNPs@rGO, NiNPs@rGO and VONPs@rGO.

e) X-ray Photo electronic spectroscopy:

To analyze the surface chemical compositions and chemical state of as-prepared catalysts, X-ray photo electronic spectroscopy has been performed. The XPS spectra of GO is discussed in chapter 2, fig. 9, which is matched with the XPS spectra of as-prepared of CuNPs@rGO. The survey spectra of as-prepared CuNPs@rGO catalyst (fig. 5 (a)), clearly signified the structure with elemental composition of carbon, oxygen and copper. As shown in Fig. 5b, the existence of two major peaks (933.5 and 953.7 eV) provide the evidence for the presence of Cu metal as Cu(0).

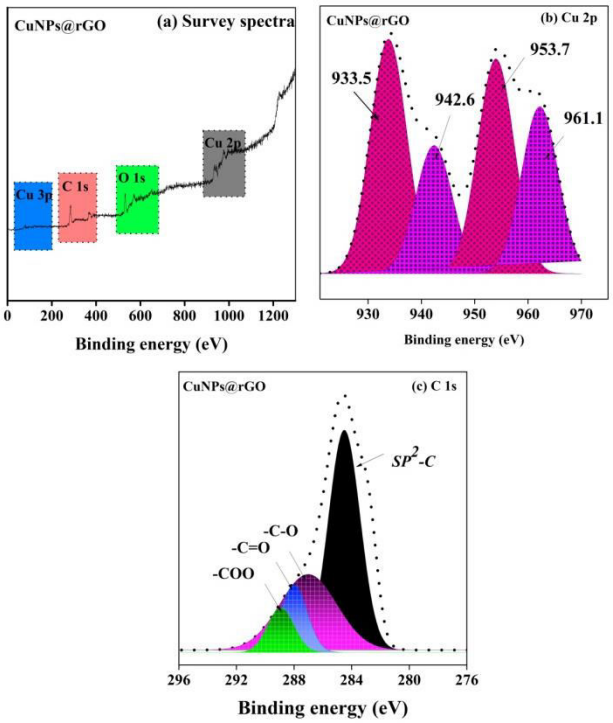

Figure 5. XPS spectra of (a) Survey spectra, (b) Cu 2P core-level spectra of CuNPs@rGO, (c) C 1s spectra of CuNPs@rGO.

Additionally, the two other peaks at 942.6 eV and 961.1 eV was also observed, indicating the existence of Cu (I) and Cu(II) salt (as l-AA was not reduced Cu absolutely) [47, 51]. Moreover, high resolution C 1s spectra of CuNPs@rGO (fig. 5c) exhibited four different prominent peaks. Whereas, the peak intensities of the as-prepared catalyst [CuNPs@rGO (fig. 5c)] observed at 287.95, 289.82 and 289.63 eV drop down remarkably, however, the existence of large intense peak of sp^2-C was observed in as-prepared CuNPs@rGO catalyst because of the restoration of new in-plane sp^2 domains, which is in good accordance with Raman spectral studies [49]. All this results confirmed the successfully the formation of CuNPs decorated on rGO nanosheet.

f) BET analysis:

The specific surface area and porous nature of GO has shown in chapter 2, fig. 11, which is matched with CuNP@rGO nanocomposite. It has been verified by BET analysis (fig. 6) and by BJH pore size distribution plot (shown in the inset fig. 6). The N_2 adsorption-desorption isotherms curve was observed similar with a

type IV curve which is a typical identification characteristic of mesoporous materials as per IUPAC classification [52]. The BET specific surface area and total pore diameter of GO (94.23 m^2g^{-1}, 40.840 Å, described in Chapter 2, fig. 11) has drop down to 40.70 m^2g^{-1} and 37.434 Å during the preparation of CuNP@rGO catalyst because of large size of CuNPs which blocks the pore diameter of GO nanostructure [53, 54].

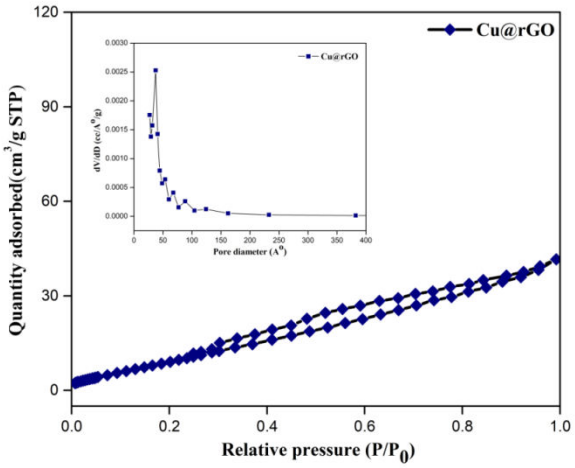

Figure 6 N_2 adsorption and desorption isotherms of CuNPs@rGO with BJH desorption pore-size distribution of the CuNPs@rGO (Inset fig.)

g) Thermogravimetric analysis

Thermogravimetric analysis was performed to evaluate the thermal stability of GO, rGO, have discuused in chapter 2, fig. 7, which are matched with CuNPs@rGO, NiNPs@rGO and VONPs@rGO.

As shown in Fig. 7, CuNPs@rGO, NiNPs@rGO and VONPs@rGO, degradation step decreased in two stages, the mass loss decreased in the first stage (7.05%, 8.96%, and 7.07%) was attributed to the removal of most of the oxygen containing functional groups by the reduction process. In the second stage, mass loss (64.83 %, 66.5% and 65.08%) was observed in the temperature range of 400-650 ^oC, assumed to be due to the pyrolysis of carbonaceous component of the graphene sheets.

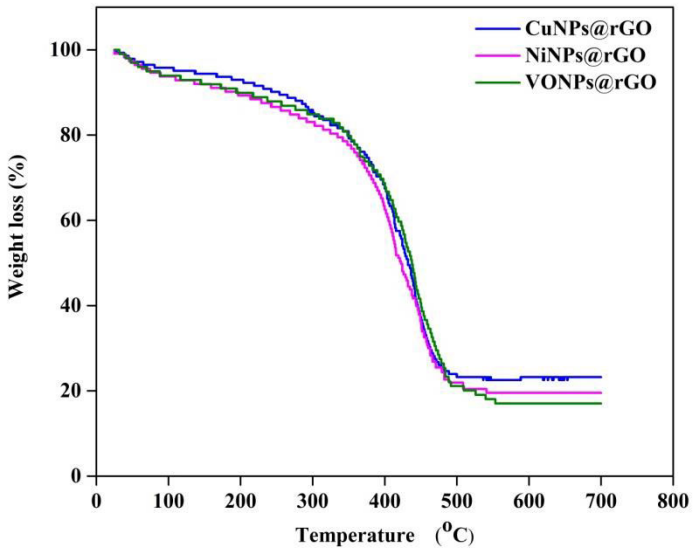

Figure 7. TG analysis of CuNPs@rGO, NiNPs@rGO, and VONPs@rGO.

[3.4] Catalytic Activity

Generally, a series of hydrogenolysis of BzA demonstrated the route of formation of absolute selective product i.e., toluene. As presented in Table 1, all the catalysts such as graphite flakes, GO, rGO, activated charcoal (AC), CuNPs@AC, CuNPs@rGO, NiNPs@rGO and VONPs@rGO were tested over the chemoselective reductive hydrogenolysis of BzA. Amongst them, CuNPs@rGO has shown the highest conversion of BzA (73.1%) and (99.9%) selectivity for toluene with 1208 h^{-1} TOF. Hence, it was preferred as a representative catalyst to acquire optimized condition by varying parameters such as mole ratio, temperature, amount of catalyst, and solvent effect.

Table 1. Catalytic performance of synthesized materials over hydrogenolysis of BzA.

Compounds	BzA conversion (%)	Selectivity of Toluene (%)	[a]TOF (h^{-1})
Graphite flakes	--	--	--
GO	6.53	60.12	--
rGO	7.02	60.88	--
Activated Carbon	2.30	58.2	--
CuNPs@rGO	73.13	99.98	1208
NiNPs@rGO	71.73	99.98	1195
VONPs@rGO	70.83	99.98	1057
CuNPs@AC	58.78	90.12	--

[a]TOF: moles of BzA converted/mole of metal × hour

Reaction condition: BzA (1 mmol), Et_3SiH (2 mmol), CuNPs@rGO (10 mg), dry ethanol (5 ml), Room temperature, 10 min.

a) Effect of Solvents:

Since solvents have a significant effect on the rate of reaction, stabilization of desired product, selectivity and catalytic activity and also on catalyst performance [55]. Researchers, in these days, are paying much attention on the influences of solvents with spent sufficient amount of time. We have explored the effect of diverse solvents like dry ethanol, methanol, and dichloromethane on the hydrogenolysis of BzA (fig. 8). It was concluded from our experimental results that, on employing methanol and dichloromethane, much less conversion was observed, which might be due to formation of a large number of by-products

because of side reaction of BzA [56]. On the other hand, dry ethanol exhibited the excellent catalytic activity by providing 73.1% conversion of BzA and 99.9% selectivity for toluene with TOF: 1208 h^{-1}. This superior efficacy of dry ethanol was believed to be owing to more positive inductive effect of methylene group on the oxygen atom making the O-H bond much weaker and consequently, the hydrogen of the ethanol would be easily available for the reduction of BzA [57]. This can also be seen in the reaction pathway which was proceed through the formation of molecular hydrogen by the interaction of dry ethanol with intermediate **species A** [56,58-59], which plays a vital role in the formation of selective product viz. toluene as depicted in (Scheme S1). As a result, dry ethanol was considered to be excellent candidate for the hydrogenolysis of BzA.

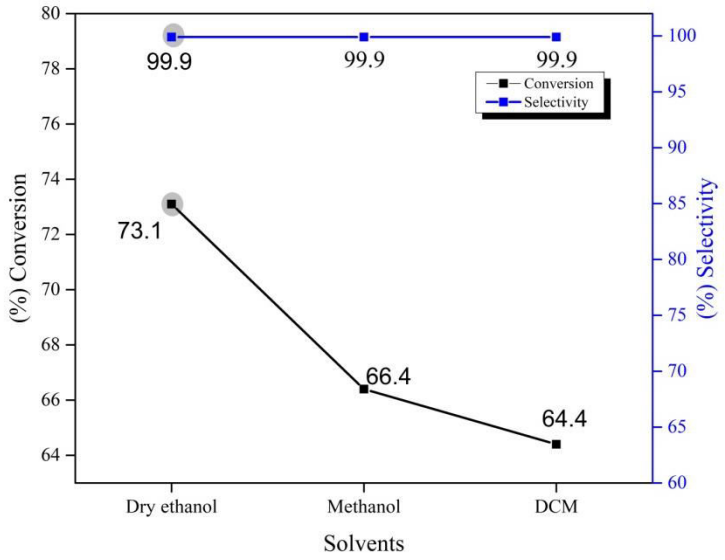

Figure 8. Impact of varying solvents

Reaction condition: BzA (1 mmol), Et_3SiH (2 mmol), CuNPs@rGO (10 mg), amount of solvent (5 ml), room temperature, 10 min.

TOFs (h^{-1}) **:** 1208 1092 1055

b) Effect of Time:

To explore the least time obligatory to achieve the highest conversion and product selectivity, the hydrogenolysis reaction has been carried out at experimentally pre-decided different time intervals by keeping other

parameters fixed. The effect of different time viz. 0.1, 1, 4, 8, 24 h on conversion and selectivity were depicted in Fig. 7. The highest % conversion of BzA and selectivity of toluene was observed at 1 h and if we further continuing the reaction, the conversion was increased with increasing time while selectivity remains intact with increasing time up to 8 h then after decreased. As a result, we have decided to set the time 1 h for further experiments.

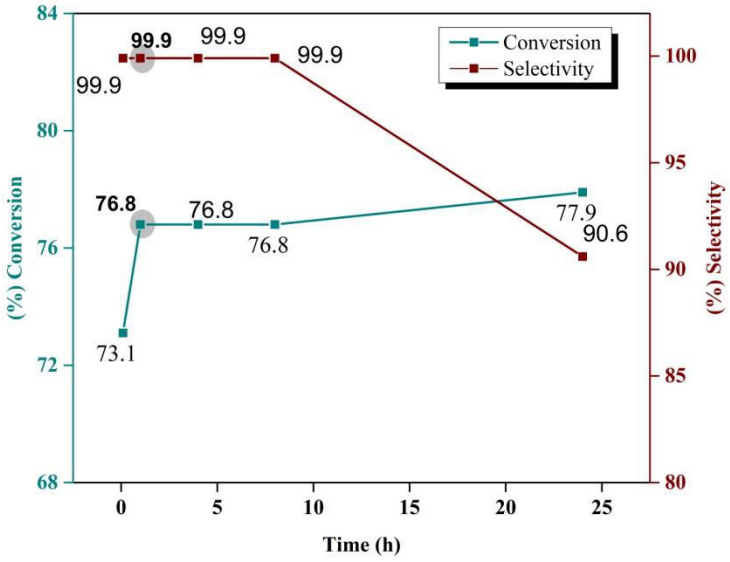

Figure 9. Impact of time

Reaction condition: BzA (1 mmol), Et_3SiH (2 mmol), CuNPs@rGO (10 mg), dry ethanol (5 ml), room temperature.

TOFs (h^{-1}) : 1208 210 52 25 8

c) Effect of mole ratio:

A series of reactions were carried out to examine the influence of concentration of hydride source to the benzyl alcohol in the catalytic hydrogenolysis of BzA. As shown in Fig. 10, four different mole ratios of BzA and Et_3SiH were taken to investigate their impact on hydrogenolysis reaction with keeping further parameters fixed. The vital effect of hydride source can be seen on this transformation, the conversion was showed an upward trend with increasing ratio of hydride. The maximum conversion of BzA (89%) was achieved at the highest ratio of Et_3SiH (1:6) but highest selectivity observed at 1:4

ratio. On continuing the increment of hydride ratio the selectivity drop-downed and this was believed to be due to over hydrogenolysis of BzA at higher hydride source. Therefore, it was clearly noticed that maximum conversion and selectivity was acquired at 1:4 ratio and was taken as optimized for the hydrogenolysis of BzA.

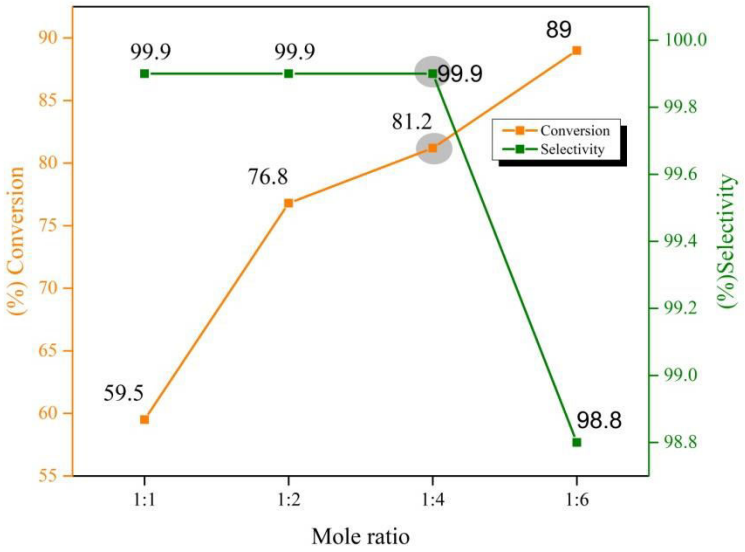

Figure 10. Impact of varying mole ratio

Reaction condition: BzA (X mmol), Et_3SiH (Y mmol) CuNPs@rGO (10 mg), dry ethanol (5 ml), room temperature, 1 h.

TOFs (h^{-1}): 163 210 222 243

d) Effect of Catalyst dosage:

Usually, for any heterogenized catalytic reaction, the amount of catalyst to be employed plays a crucial role. Four different amounts of CuNPs@rGO catalyst such as 10, 25, 50, and 60 mg were investigated for the hydrogenolysis of BzA (fig. 11). Maximum conversion of BzA was observed with 10 mg of catalyst and no significant change in the conversion of BzA was examined on increasing the catalyst amount from 10 to 60 mg. Consequently, the quantity of the catalyst was considered to be 10 mg for further exploration of optimization of remaining parameters [60].

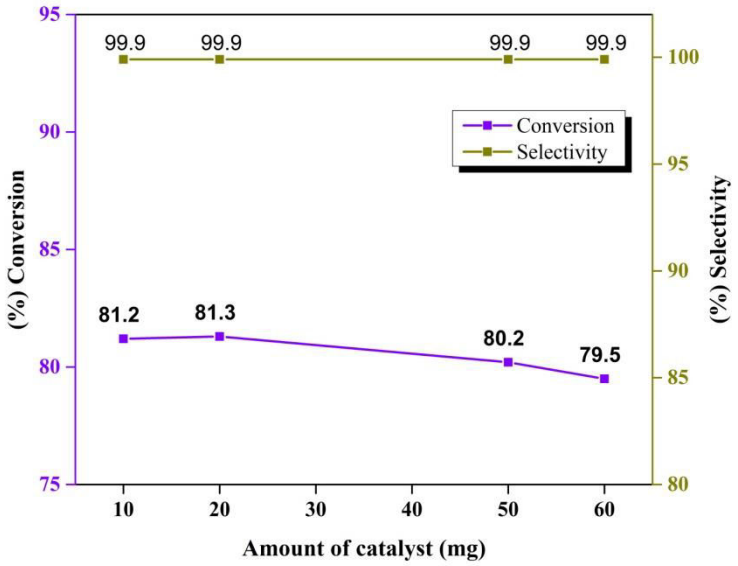

Figure 11. Impact of amount of catalyst.

Reaction condition: BzA (1 mmol), Et_3SiH (4 mmol), dry ethanol (5 ml), room temperature, 1 h.

TOFs (h^{-1}): 222 111 44 36

e) Effect of Temperature:

To probe the reaction temperature at which highest conversion and selectivity can acquire the hydrogenolysis of BzA was conducted at different temperatures i.e. (Room temperature) RT, 35 and 45 ^{o}C. It was obvious from Fig. 12 that almost no rise was observed in the conversion with increasing temperature from RT to 45 °C. Hence, RT was considered as the optimized temperature for further investigation and is being not harmful to the environment, considered as a greener approach.

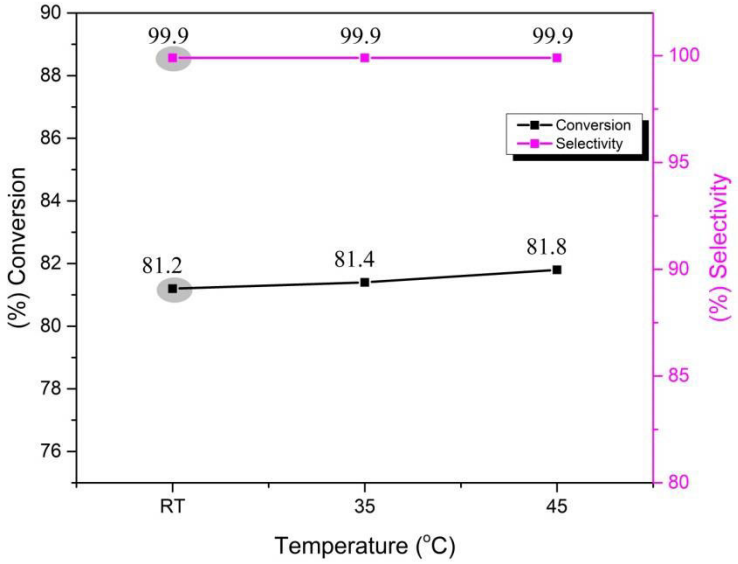

Figure 12. Impact of varying temperature.

Reaction condition: BzA (1 mmol), Et_3SiH (4 mmol) CuNPs@rGO (10 mg), dry ethanol (5 ml), 1h.

TOFs (h^{-1}): 222 223 224

[3.5] Catalytic hydrogenolysis of various benzyl alcohol derivatives

Under the optimized reaction conditions, we have tested the efficacy of CuNPs@rGO catalyst over hydrogenolysis reaction with different benzyl alcohol derivatives such as benzyl alcohol, 4-methoxy benzyl alcohol and 4-methyl benzyl alcohol are depicted in Table 2.

Table 2. Hydrogenolysis of various benzyl alcohol derivatives.

Entry	Subtracts	Product	Conversion (%)	Selectivity (%)
1	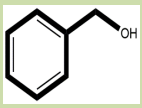	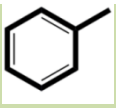	81.2	99.9
2	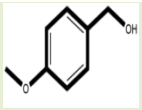	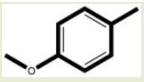	74.1	80.2
3	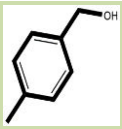	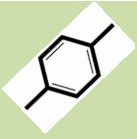	72.6	79.1

Reaction condition: BzA derivatives (1 mmol), Et_3SiH (4 mmol) CuNPs@rGO (10 mg), dry ethanol (5 ml), 1h.

[3.6] Catalytic assessment

Catalytic hydrogenolysis of BzA using varying homogeneous and/or heterogeneous systems (Table 3) has been studied previously by some other groups as discussed here. David Raju Burri et al. [61] have reported hydrogenolysis of BzA catalyzed by various homogeneous catalysts system such as 1Cu/MgO, 3Cu/MgO, 5Cu/MgO and 7Cu/MgO using H_2 molecule as hydride source. Amongst all these homogeneous systems, 7Cu/MgO was proven better catalyst with 89% conversion but only 22% product selectivity. Silica supported Ru catalyst was developed by Chung-Sung Tan and co-workers [62] and investigated over hydrogenolysis of BzA. This system achieved the highest % conversion of BzA (86%) with 83.6% toluene selectivity. Raney nickel in refluxing 2- propanol was taken as a catalyst for hydrogenolysis of BzA by Robert C. Mebane and co-workers [63] achieving 87% yield of toluene with some other by-products. Christopher McRae et al. [64] used Lewis acid catalyst tris(pentafluorophenyl)borane ($B(C_6F_5)_3$) in the presence of either diethylsilane or n-butylsilane as a reducing agent for reduction of alcohol. They achieved 97% yield of product in presence of diethylsilane whereas, use of n-butylsilane resulted in a 41% yield of the desired product. Serge Kaliaguine et al. [56] have studied numerous Pd^0 based heterogeneous catalysts viz. SiliaCat Pd^0, Pd/polyethylenimine/SiO_2, Pd/SiO_2, and Pd/C for hydrogenolysis of BzA. Amongst them, glassy hybrid spherical SiliaCat Pd^0 catalyst is highly mediator under a mild reaction condition because of it exhibited 100% conversion of BzA with 97% selectivity of toluene. Maryam Mirza-Aghayan and his group focused on reduction of BzA using Pd nanoparticles supported on rGO as an efficient catalyst with using dry ethanol used as a solvent [36]. In this work, they have observed 99% yield of the product. Our own results show that, when CuNPs@rGO was used for hydrogenolysis of BzA with Et_3SiH as a reducing agent under optimized reaction condition gave 81.2% BzA conversion with selective formation of 99.9% toluene. If we observe other work carefully (Table

3), in some of the work, higher conversion and selectivity was achieved but at the cost of environmental and economical impact. One can find almost all the catalysts used so far for hydrogenolysis reaction of BzA as mentioned above were costlier, time-consuming, and/or tedious catalyst separation method too. On the other hand, CuNPs@rGO is a cheaper, highly stable, re-usable, and environmentally benign catalyst with achieving higher conversion of BzA at ambient temperature.

Table 3. Comparison between reported catalytic systems and CuNPs@rGO for Hydrogenolysis of BzA.

Entry	Catalyst	Hydride Sources	Solvent/ (Temperature (°C))	Yield/ Selectivity (%)	BzA Conversion (%)	Ref.
1	Cu/MgO	H_2	--/(280)	22	89	[61]
2	Ru/MCM-41	H_2	Water/(50)	82.6	86	[62]
3	Raney Ni	2-propanol	--	87		[63]
4	$B(C_6F_5)_3$	n-butylsilane or diethylsilane	CH_2Cl_2	97 41		[64]
5	SiliaCat Pd^0	H_2	MeOH/(70)	97	100	[55]
6	Pd@rGO	Et_3SiH	Dry ethan	99		[36]

			ol/(RT)			
7	CuNPs@rGO	Et_3SiH	Dry ethanol/(RT)	99.9	81.2	Present work

[3.7] Catalytic mechanism

In the beginning of the cycle, the interaction of Et_3SiH with CuNPs@rGO as a representative catalyst generates an intermediate **species A** (Scheme 1), which further reacts with EtOH at room temperature forming molecular hydrogen and ethoxytriethylsilane (Et_3SiOEt) as a by-product. In the next step, the active hydrogen species generated was cleaved to form two metal-hydride bonds by chemisorption on the surface of metal (**Species B**). Furthermore, addition of BzA gets react with the cleaved hydrogen forming "four centre mechanism" (FCM) (**Species C**). In the final elimination step, C-O bond broken down easily amongst the C-H and C-O bond formed in the intermediary steps as the bond energy of C-H bond is higher than C-O giving toluene as the selective product. [58]

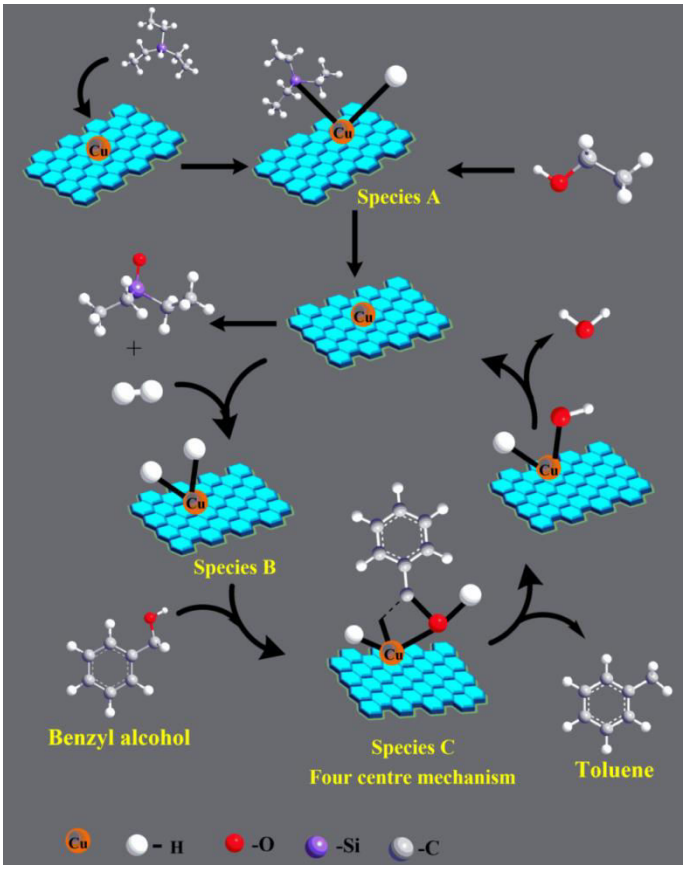

Scheme 1. A plausible catalytic cycle for the hydrogenolysis of BzA using CuNPs@rGO catalyst.

[3.8] Recyclability Test

Since the activity and stability of the as-prepared catalyst is one of the most significant factors in the field of catalysis, we have examined recyclability test (Fig. 13) of CuNPs@rGO catalyst for the hydrogenolysis of BzA under the optimized reaction conditions. After performing the catalytic reaction, the catalyst was filtered by the sintered funnel and washed with acetonitrile after each run. The catalyst was recovered carefully in order to ensure that there was no loss of the catalyst. As shown in Fig. 13, the catalyst was successfully run for six consecutive times, however, after 5^{th} run, the conversion of BzA was decreased up to 76% in the 6^{th} cycle.

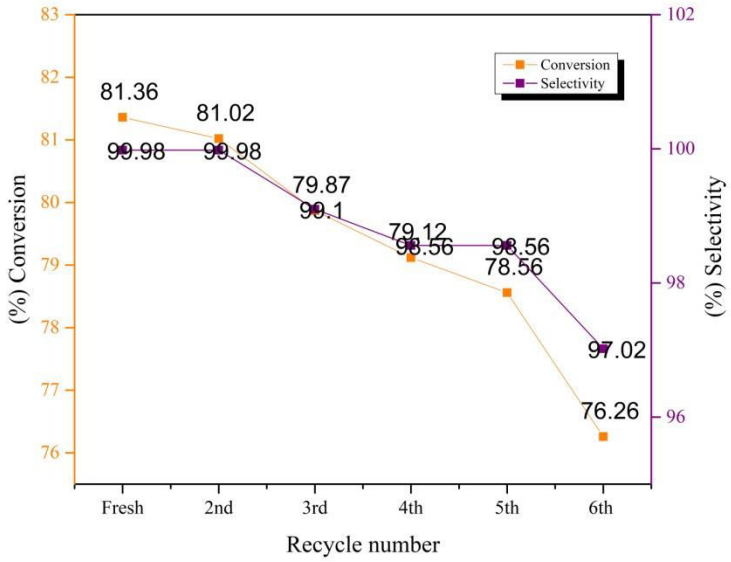

Figure 13. Recyclability test of CuNPs@rGO catalyst over hydrogenolysis of BzA.

Reaction condition: BzA (1 mmol), Et_3SiH (4 mmol) CuNPs@rGO (10 mg), dry ethanol (5 ml), room temperature, 1 h.

[3.9] Conclusions

In concluding remarks, we have established an eco-friendly approach for *in situ* synthesis of MNPs embedded on reduced graphene oxide (MNPs@rGO) nanocatalysts for the first time. MNPs@rGO accorded notable catalytic activity and selectivity in the hydrogenolysis of BzA. Amongst them, CuNPs@rGO demonstrated significantly enhanced catalytic efficacy leading to 81.2% BzA conversion (TOF: 222 h^{-1}) with exceptional 99.9% toluene selectivity. In addition to this, CuNPs@rGO catalyst could be easily recycled and reused without momentous loss of activity in the fifth cycles test. The proposed reaction pathway for the aforementioned reaction would involve *in situ* generation of molecular hydrogen, accompanied by chemisorption to architect two metal-hydride bonds and at the later stage formation of toluene as the selective product via cleavage of C-O bond. These MNPs@rGO nanocatalysts are expected to pave the way of new opportunity in the growth of rationally active and recyclable heterogeneous multifunctional catalysts for state-of-the-art chemical transformations.

[3.10] References

[1] G. Centi, S. Perathoner, *Catal. Today.* **77**, 287 (2003).

[2] J.H. Clark, D.J. Macquarrie, *Org. Process Res. Dev.* **1**, 149 (1997).

[3] Y. Wang, X. Wang, M. Antonietti, *Angew. Chemie Int. Ed.* **51**, 68 (2012).

[4] A. Dhakshinamoorthy, M. Alvaro, H. Garcia, *Catal. Sci. Technol.* **1**, 856 (2011).

[5] D. Habibi, A.R. Faraji, M. Arshadi, J.L.G. Fierro, *J. Mol. Catal. A Chem.* **372**, 90 (2013).

[6] M. Maurya, A. Kumar, J. Costa Pessoa, Coord. Chem. Rev. **255**, 2315 (2011).

[7] A. Zapf, M. Beller, *Top. Catal.* **19**, 101 (2002).

[8] M. Yoon, R. Srirambalaji, K. Kim, *Chem. Rev.* **112**, 1196 (2012).

[9] P. Sudarsanam, L. Katta, G. Thrimurthulu, B.M. Reddy, *J. Ind. Eng. Chem.* **19**, 1517 (2013).

[10] K.-H. Kim, S.-K. Ihm, *J. Hazard. Mater.* **186**, 16 (2011).

[11] A. Kajbafvala, H. Ghorbani, A. Paravar, J.P. Samberg, E. Kajbafvala, S.K. Sadrnezhaad, *Superlattices Microstruct*. **51**, 512 (2012).

[12] H. Sakurai, T. Tsukuda, T. Hirao, *J. Org. Chem.* **67**, 2721 (2002).

[13] X. Chen, Y. Hou, H. Wang, Y. Cao, J. He, *J. Phys. Chem. C.* **112**, 8172 (2008).

[14] A. Biffis, M. Zecca, M. Basato, *Eur. J. Inorg. Chem.* **2001**, 1131 (2001).

[15] R.B. Bedford, U.G. Singh, R.I. Walton, R.T. Williams, S.A. Davis, *Chem. Mater.* **17**, 701 (2005).

[16] C.K. Modi, S. Panwala, R. Vithalani, D. Patel, *J. Porous Mater.* **25**, 871 (2018).

[17] J. Baloyi, T. Ntho, J. Moma, *J. Porous Mater.* **26**, 583 (2019).

[18] A.S. Singh, U.B. Patil, J.M. Nagarkar, *Catal. Commun.* **35**, 11 (2013).

[19] C. K. Modi, R. Vithalani, D. Patel. In *Graphene Oxide Advances in Research and Applications,* A. Mishra, D. Pathania (Ed.), pp. 217-244, NOVA Science Publishers, USA (2018)

[20] S. Thakur, N. Karak, *Carbon*, **94***,* 224 (2015).

[21] R. Vithalani, D. Patel, C. K. Modi, N. N. Som, P. K. Jha, S.R. Kane, *Diam. Relat. Mater.* **90**, 154 (2018).

[22] R. Vithalani, D. S. Patel, C. K. Modi, V. Sharma, P. K. Jha, *Appl. Organomet. Chem.* (2020); doi.org/10.1002/aoc.5500.

[23] A.K. Geim, K.S. Novoselov, *Nat. Mater.* **6**, 183 (2007).

[24] A.K. Geim, *Science* **324**, 1530 (2009).

[25] X.-C. Zheng, N. Li, S. Jiang, M. Wu, G.-P. Zheng, *J. Porous Mater.* **26**, 723 (2019).

[26] D. Patel, R. Vithalani, C. K. Modi, *New J. Chem*. **44**, 2868 (2020).

[27] M. Salavati-Niasari, F. Davar, M.R. Loghman-Estarki, *J. Alloys Compd.* **481**, 776 (2009).

[28] M. Salavati-Niasari, M. Dadkhah, F. Davar, *Inorganica Chim. Acta.* **362**, 3969 (2009).

[29] H. Safajou, H. Khojasteh, M. Salavati-Niasari, S. Mortazavi-Derazkola, *J. Colloid Interface Sci.* **498**, 423 (2017).

[30] F. Mohandes, M. Salavati-Niasari, *Ultrason. Sonochem.* **20**, 354 (2013).

[31] M. Mahdiani, F. Soofivand, F. Ansari, M. Salavati-Niasari, *J. Clean. Prod.* **176**, 1185 (2018).

[32] M. Esmaeili-Zare, M. Salavati-Niasari, A. Sobhani, *Ultrason. Sonochem.* **19**, 1079 (2018).

[33] F. Davar, M. Salavati-Niasari, N. Mir, K. Saberyan, M. Monemzadeh, E. Ahmadi, *Polyhedron*. **29**, 1747 (2010).

[34] Z. Ji, Y. Wang, X. Shen, H. Ma, J. Yang, A. Yuan, H. Zhou, *J. Colloid Interface Sci.* **487**, 223 (2017).

[35] M. Mirza-Aghayan, R. Boukherroub, M. Rahimifard, *Tetrahedron Lett.* **50**, 5930 (2009).

[36] M. Mirza-Aghayan, M. Molaee Tavana, R. Boukherroub, *Catal. Commun.* **69**, 97 (2015).

[37] M.M. Nigra, J.-M. Ha, A. Katz, *Catal. Sci. Technol.* **3**, 2976 (2013).

[38] Y. Junejo, A. Güner, A. Baykal, *Appl. Surf. Sci.* **317**, 914 (2014).

[39] C. Chatgilialoglu, C. Ferreri, M. Lucarini, *J. Org. Chem.* **58**, 249 (1993).

[40] E. Keinan, N. Greenspoon, *J. Am. Chem. Soc.* **108**, 7314 (1986).

[41] I. Ojima, T. Kogure, Y. Nagai, *Tetrahedron Lett*. **14**, 2475 (1973).

[42] L.Y. Chan, J.S.K. Lim, S. Kim, *Synlett.* **2011**, 2862 (2011).

[43] M. Egi, T. Kawai, M. Umemura, S. Akai, *J. Org. Chem.* **77**, 7092 (2012).

[44] M. Mirza-Aghayan, R. Boukherroub, M. Bolourtchian, M. Rahimifard, *J. Organomet. Chem.* **692**, 5113 (2007).

[45] M. Mirza-Aghayan, R. Boukherroub, M. Rahimifard, *J. Organomet. Chem.* **693**, 3567 (2008).

[46] B. Paulchamy, G. Arthi, B.D. Lignesh, *J Nanomed Nanotechnol.* **6**, 253 (2015).

[47] N. Hussain, P. Gogoi, V.K. Azhaganand, M. V Shelke, M.R. Das, *Catal. Sci. Technol.* **5**, 1251 (2015).

[48] C. Zhang, M. Chen, X. Xu, L. Zhang, L. Zhang, F. Xia, X. Li, Y. Liu, W. Hu, J. Gao, *Nanotechnology*. **25**, 135707 (2014).

[49] G. Darabdhara, P.K. Boruah, P. Borthakur, N. Hussain, M.R. Das, T. Ahamad, S.M. Alshehri, V. Malgras, K.C.-W. Wu, Y. Yamauchi, *Nanoscale*. **8**, 8276 (2016).

[50] Y. Yang, Z.-H. Lu, Y. Hu, Z. Zhang, W. Shi, X. Chen, T. Wang, *RSC Adv*. **4**, 13749 (2014).

[51] P. Mondal, A. Sinha, N. Salam, A. S. Roy, N. R. Jana, S. M. Islam, *RSC Adv*. **3**, 5615 (2013).

[52] Y. Li, R. Zhang, X. Tian, C. Yang, Z. Zhou, *Appl. Surf. Sci.* **369**, 11 (2016).

[53] Y. Li, Z. Li, P.K. Shen, *Adv. Mater.* **25**, 2474 (2013).

[54] K.B. Babitha, J. Jani Matilda, A. Peer Mohamed, S. Ananthakumar, *RSC Adv.* **5**, 50223 (2015).

[55] C. Reichardt, T. Welton, Wiley, 2011.

[56] V. Pandarus, R. Ciriminna, G. Gingras, F. Béland, M. Pagliaro, S. Kaliaguine, *ChemistryOpen*. **7**, 80 (2018).

[57] J. Zhang, K. Dong, W. Luo, and H. Guan, *ACS Omega* **3**, 6206 (2018).

[58] M. Mirza-Aghayan, R. Boukherroub, M. Bolourtchian, M. Hosseini, *Tetrahedron Lett.* **44**, 4579 (2003).

[59] M. Mirza-Aghayan, R. Boukherroub, M. Bolourtchian, *Appl. Organomet. Chem.* **20**, 214 (2006).

[60] H. W. Lee, H. T. Dang, H. Kim, U. Lee, J.-M. Ha, J. Jae, M. Cheong, H. Lee, *J. Catal*. **374**, 230 (2019).

[61] R.K. Marella, C.K.P. Neeli, S.R.R. Kamaraju, D.R. Burri, *Catal. Sci. Technol*. **2**, 1833 (2012).

[62] H.-W. Lin, C.H. Yen, C.-S. Tan, *Green Chem*. **14**, 682 (2012)

[63] B.H. Gross, R.C. Mebane, D.L. Armstrong, *Appl. Catal. A Gen.* **219**, 281 (2001).

[64] R.D. Nimmagadda, C. McRae, *Tetrahedron Lett.* **47**, 5755 (2006).